

REPORT DOCUMENTATION PAGEForm Approved
OMB No. 0704-0188

Public reporting burden for this collection of information is estimated to average 1 hour per response, including the time for reviewing instructions, searching existing data sources, gathering and maintaining the data needed, and completing and reviewing this collection of information. Send comments regarding this burden estimate or any other aspect of this collection of information, including suggestions for reducing this burden to Department of Defense, Washington Headquarters Services, Directorate for Information Operations and Reports (0704-0188), 1215 Jefferson Davis Highway, Suite 1204, Arlington, VA 22202-4302. Respondents should be aware that notwithstanding any other provision of law, no person shall be subject to any penalty for failing to comply with a collection of information if it does not display a currently valid OMB control number. PLEASE DO NOT RETURN YOUR FORM TO THE ABOVE ADDRESS.

1. REPORT DATE (DD-MM-YYYY)

13 February 2003

2. REPORT TYPE

Technical Paper

3. DATES COVERED (From - To)**4. TITLE AND SUBTITLE**Synthesis and Characterization of the trans-IO₂F₅²⁻ Dianion**5a. CONTRACT NUMBER****5b. GRANT NUMBER****5c. PROGRAM ELEMENT NUMBER****6. AUTHOR(S)**Jerry A. Boatz, William J. Casteel, Jr., Karl O. Christe, David A. Dixon, Michael Gerken,
Robert Z. Gnann, Helene P. A. Mercier, Gary J. Schrobilgen**5d. PROJECT NUMBER
DARP****5e. TASK NUMBER
A205****5f. WORK UNIT NUMBER****7. PERFORMING ORGANIZATION NAME(S) AND ADDRESS(ES)**Air Force Research Laboratory (AFMC)
AFRL/PRSP
10 E. Saturn Blvd.
Edwards AFB, CA 93524-7680**8. PERFORMING ORGANIZATION
REPORT NUMBER**

AFRL-PR-ED-TP-2003-036

9. SPONSORING / MONITORING AGENCY NAME(S) AND ADDRESS(ES)Air Force Research Laboratory (AFMC)
AFRL/PRS
5 Pollux Drive
Edwards AFB CA 93524-7048**10. SPONSOR/MONITOR'S
ACRONYM(S)****11. SPONSOR/MONITOR'S
NUMBER(S)
AFRL-PR-ED-TP-2003-036****12. DISTRIBUTION / AVAILABILITY STATEMENT**

Approved for public release; distribution unlimited.

13. SUPPLEMENTARY NOTES**14. ABSTRACT**

20030320 049

15. SUBJECT TERMS**16. SECURITY CLASSIFICATION OF:****17. LIMITATION
OF ABSTRACT****18. NUMBER
OF PAGES****19a. NAME OF RESPONSIBLE
PERSON
Sheila Benner****a. REPORT****b. ABSTRACT****c. THIS PAGE**

Unclassified

Unclassified

Unclassified

A

**19b. TELEPHONE NUMBER
(include area code)
(661) 275-5693**Standard Form 298 (Rev. 8-98)
Prescribed by ANSI Std. Z39.18

FILE

MEMORANDUM FOR PRS (In-House Publication)

FROM: PROI (STINFO)

11 Feb 2003

SUBJECT: Authorization for Release of Technical Information, Control Number: **AFRL-PR-ED-TP-2003-036**

55364 Jerry A. Boatz (AFRL/PRSP); William J. Casteel, Jr.; Karl O. Christe; David A. Dixon; Michael Gerken; Robert Z. Gnann; Helene P.A. Mercier, and Gary J. Schrobilgen "Synthesis and Characterization of the *trans*-IO₂F₃²⁻ Dianion"

Journal of the American Chemical Society

(Statement A)

Synthesis and Characterization of the *trans*-IO₂F₅²⁻ Dianion

Jerry A. Boatz,[†] William J. Casteel, Jr.,[‡] Karl O. Christe,^{†,*} David A. Dixon,[§] Michael Gerken,^{‡,*} Robert Z. Gnann,[‡] Helene P. A. Mercier,[‡] and Gary J. Schrobilgen,^{‡,*}

Contribution from the Loker Hydrocarbon Research Institute, University of Southern California, University Park, Los Angeles, California 90089, Air Force Research Laboratory, Edwards Air Force Base, California 93524, Department of Chemistry, McMaster University, Hamilton, Ontario L8S 4M1, Canada, and Fundamental Sciences Division, Pacific Northwest National Laboratory, Richland, Washington 99352

Abstract

The combination of CH₃CN solutions of [N(CH₃)₄][F] and a mixture of *cis*- and *trans*-[N(CH₃)₄][IO₂F₄] produces the novel *trans*-IO₂F₅²⁻ anion. Under the given conditions, only the *trans*-IO₂F₄⁻ anion acts as a fluoride ion acceptor, thus allowing the separation of isomerically pure, soluble *cis*-IO₂F₄⁻ from insoluble *trans*-IO₂F₅²⁻. The *trans*-IO₂F₅²⁻ and *cis*-IO₂F₄⁻ anions were characterized by infrared and Raman spectroscopy and theoretical calculations at the LDFT and HF levels of theory. The *trans*-IO₂F₅²⁻ anion has a pentagonal-bipyramidal geometry with the two oxygen atoms occupying the axial positions. It represents the first example of a heptacoordinated main group AO₂X₅ species and completes the series of pentagonal-bipyramidal iodine fluoride and oxofluoride species. The geometries of the pentagonal-bipyramidal series IO₂F₅²⁻, IOF₅²⁻, IF₅²⁻, IOF₆⁻, IF₆⁻, and IF₇, and the corresponding octahedral series IO₂F₄⁻, IOF₄⁻, IF₄⁻, IOF₅, IF₅, and IF₆⁺ were calculated by identical methods. It is shown how the ionic charge, the oxidation state of the central atom, the coordination number, and the replacement of fluorine ligands by either an oxygen ligand or a free valence electron pair influence the structures and bonding of these species.

DISTRIBUTION STATEMENT A
Approved for Public Release
Distribution Unlimited

Introduction

Main-group fluorides and oxofluorides offer a unique opportunity to study high coordination numbers, the steric influence and relative repulsion effects of fluorine, oxygen and sterically active free valence electron pairs, and fluxionality. Of particular interest in this respect is the coordination number seven. Although heptacoordinated species can exist in three different conformations of similar energy, i. e., either as a monocapped octahedron, a monocapped trigonal prism, or a pentagonal bipyramid,^{1,2} main group elements generally prefer pentagonal bipyramidal structures^{3,4} since this geometry results in a better overlap of the ligand orbitals with the *s* and *p* orbitals of the central atom. As part of our systematic studies of heptacoordination, the structures of main group AF_5XY species have been studied where X and Y represent either fluorine or oxygen ligands or sterically active free valence electron pairs (E).^{3,5-14} Structures for all members of this series have been established, except for the AO_2F_5 case. In this paper, the preparation and structure of the $IO_2F_5^{2-}$ dianion, the first example of a main-group AO_2F_5 species, is reported.

Experimental

Materials and Apparatus. All volatile materials were handled in either a Pyrex vacuum line equipped with Kontes or J. Young glass-Teflon valves or a stainless steel, Teflon-FEP vacuum line.¹⁵ Nonvolatile materials were handled in the dry nitrogen atmosphere of a glove box.

The solvents, CH_3CN (Baker, HPLC Grade) and anhydrous HF (Harshaw) were dried by storage over P_2O_5 and BiF_5 ,¹⁶ respectively, and distilled prior to their use. The syntheses of $[N(CH_3)_4][F]^{17}$ and $IO_2F_3^{18}$ have been described previously.

Preparation of $[N(CH_3)_4][IO_4]$. Tetramethylammonium metaperiodate, $[N(CH_3)_4][IO_4]$, was prepared either by a literature method¹⁹ or by the following metathesis reaction. Approximately 30 mL of a 0.76 M aqueous solution of $[N(CH_3)_4][Cl]$ (Fluka Chemika, 98%)

(22.80 mmol) was slowly added, with stirring, to 40 mL of aqueous $[\text{Na}][\text{IO}_4]$ (Matheson Coleman & Bell, 99.8%) (22.77 mmol). A white precipitate formed almost immediately and the resulting mixture was stirred in an ice water bath for 30 min. The $[\text{N}(\text{CH}_3)_4][\text{IO}_4]$ precipitate was filtered off, washed with ice cold water, and dried for 15 h at 88 °C in a dynamic vacuum. $[\text{N}(\text{CH}_3)_4][\text{IO}_4]$ was obtained in a yield of 53.7 % (3.2643 g). Infrared and Raman spectroscopy of the product showed no detectable amounts of water.

Preparation of $[\text{N}(\text{CH}_3)_4][\text{IO}_2\text{F}_4]$. Tetramethylammonium tetrafluoroperiodate was prepared by analogy with a previously published²⁰ method. In the drybox, $[\text{N}(\text{CH}_3)_4][\text{IO}_4]$ (2.995 mmol) was loaded into a 20 cm long, 1/2-in. o.d. Teflon-FEP tube that was closed by a Kel-F valve. On the metal line, anhydrous HF (3.4 mL) was distilled onto the $[\text{N}(\text{CH}_3)_4][\text{IO}_4]$. The mixture was allowed to warm to room temperature, giving a colorless solution, and agitated for 3 days on a mechanical shaker. The HF and H_2O were pumped off between 0 °C and 45 °C for 14 h. Fresh anhydrous HF was distilled onto the sample and the tube was agitated for an additional 2 days, followed by removal of the solvent in a dynamic vacuum to give $[\text{N}(\text{CH}_3)_4][\text{IO}_2\text{F}_4]$ in 96.8% yield in the form of a white, crystalline solid. The purity was verified by its low-temperature Raman spectrum, which showed the presence of a mixture of $[\text{N}(\text{CH}_3)_4][\text{cis-IO}_2\text{F}_4]$ and $[\text{N}(\text{CH}_3)_4][\text{trans-IO}_2\text{F}_4]$ (*cis-IO*₂F₄⁻: 207 (3), 235 (<0.5), 330 (35), 366 sh, 394 (19), $\nu_4(\text{A}_1)$; 560 (24), $\nu_3(\text{A}_1)$; 610 (74), $\nu_2(\text{A}_1)$; 847 (75), $\nu_1(\text{A}_1)$; and 870 (13), 880 sh, cm^{-1} , $\nu_{12}(\text{B}_2)$; *trans-IO*₂F₄⁻: 251 (5), $\nu_6(\text{B}_{2g})$; 380 (41), $\nu_8(\text{E}_g)$; 560 (24), $\nu_5(\text{B}_{1g})$; 571 (65), $\nu_2(\text{A}_{1g})$; and 813 (100) cm^{-1} , $\nu_1(\text{A}_{1g})$). Fluorine-19 NMR spectroscopy of $[\text{N}(\text{CH}_3)_4][\text{IO}_2\text{F}_4]$ in HF solution indicated an approximate *cis*- to *trans*-isomer ratio of 70:30.

Alternatively, $[\text{N}(\text{CH}_3)_4][\text{IO}_2\text{F}_4]$ was prepared from IO_2F_3 and $[\text{N}(\text{CH}_3)_4][\text{F}]$. In a typical synthesis, IO_2F_3 (10.774 mmol) was condensed into a 3/8-in. o.d. Teflon-FEP reaction tube equipped with a Kel-F valve, and 5 mL of anhydrous HF was condensed onto the solid at -196

°C. The IO_2F_3 completely dissolved upon warming to room temperature and agitation. The solution was transferred into a drybox and frozen in a $-196\text{ }^\circ\text{C}$ cold well, and $[\text{N}(\text{CH}_3)_4][\text{F}]$ (11.050 mmol) was added. The reactor was removed from the drybox and warmed to room temperature resulting in a colorless solution. Removal of the HF for several hours in a dynamic vacuum gave colorless, friable, microcrystalline $[\text{N}(\text{CH}_3)_4][\text{IO}_2\text{F}_4]$ (10.854 mmol). Its purity was established by Raman spectroscopy. **CAUTION: The condensation of IO_2F_3 onto frozen CH_3CN solutions can result in detonations when the mixtures are warmed to the melting point of the solvent and must be avoided.**

Preparation of $[\text{N}(\text{CH}_3)_4]_2[\text{IO}_2\text{F}_5]$. Inside the drybox, $[\text{N}(\text{CH}_3)_4][\text{IO}_2\text{F}_4]$ (1.853 mmol) was added to one arm of a flamed-out, H-shaped glass reaction vessel equipped with a Young valve on each side and one separating the two arms. A stoichiometric amount of $[\text{N}(\text{CH}_3)_4][\text{F}]$ (1.882 mmol) was added to the other arm of the reaction vessel. Anhydrous CH_3CN was condensed at $-196\text{ }^\circ\text{C}$ into both arms, and the reactor was warmed to $-30\text{ }^\circ\text{C}$. The CH_3CN solution of $[\text{N}(\text{CH}_3)_4][\text{F}]$ was transferred into the arm of the reaction vessel containing the $[\text{N}(\text{CH}_3)_4][\text{IO}_2\text{F}_4]$ solution. The mixture was stirred at $-30\text{ }^\circ\text{C}$ for 2 h using a magnetic stir bar. The CH_3CN solvent was pumped off over a period of 16 h while slowly warming from -30 to $0\text{ }^\circ\text{C}$, yielding 0.7970 g of a fine, white powder consisting of $[\text{N}(\text{CH}_3)_4]_2[\text{IO}_2\text{F}_5]$, $[\text{N}(\text{CH}_3)_4][\text{F}]$, and $[\text{N}(\text{CH}_3)_4][\text{cis-IO}_2\text{F}_4]$.

Inside the drybox, part of the above described $[\text{N}(\text{CH}_3)_4]_2[\text{IO}_2\text{F}_5]$ / $[\text{N}(\text{CH}_3)_4][\text{F}]$ / $[\text{N}(\text{CH}_3)_4][\text{cis-IO}_2\text{F}_4]$ mixture (0.3433 g) was loaded into one arm of the H-shaped reaction vessel. Anhydrous CH_3CN was distilled onto the mixture in a static vacuum at $-196\text{ }^\circ\text{C}$. The mixture was allowed to warm to $-20\text{ }^\circ\text{C}$, was agitated, and then allowed to settle. After 2 h, the CH_3CN solution was decanted into the other arm of the reaction vessel, and the solvent was distilled back onto the solid residue. Washing of the solid was repeated ten more times before the CH_3CN solvent was

pumped off on the glass vacuum line for 12 h while warming from -30 to 25 °C to yield 0.1382 g of a fine, white powder that consisted, based on its weight and vibrational spectra, of 75 weight % $[\text{N}(\text{CH}_3)_4]_2[\text{IO}_2\text{F}_5]$ and 25 weight % $[\text{N}(\text{CH}_3)_4][\text{cis-IO}_2\text{F}_4]$.

Alternatively, a previously described Teflon-FEP metathesis apparatus²¹ was loaded in the dry box with $[\text{N}(\text{CH}_3)_4][\text{F}]$ (2.58 mmol) and $[\text{N}(\text{CH}_3)_4][\text{IO}_2\text{F}_4]$ (2.01 mmol). On a glass vacuum line, approximately 10 mL CH_3CN was condensed onto the solid at -196 °C. After melting of the CH_3CN solvent at -31 °C, the reaction mixture was kept at -31 °C for 2 h and periodically stirred resulting in the formation of copious amounts of white solid. The apparatus was inverted and the reaction mixture was quickly pressure filtered, followed by removal of the CH_3CN in a dynamic vacuum at ambient temperature. Inside the dry box, the apparatus was disassembled and 0.550 g of a white solid from the filter cake (containing $[\text{N}(\text{CH}_3)_4]_2[\text{IO}_2\text{F}_5]$, $[\text{N}(\text{CH}_3)_4][\text{cis-IO}_2\text{F}_4]$, and trace amounts of $[\text{N}(\text{CH}_3)_4][\text{trans-IO}_2\text{F}_4]$) and 0.250 g of a white filtrate residue, containing $[\text{N}(\text{CH}_3)_4][\text{F}]$ and isomerically pure $[\text{N}(\text{CH}_3)_4][\text{cis-IO}_2\text{F}_4]$, were collected.

In another modification, clear solutions of $[\text{N}(\text{CH}_3)_4][\text{F}]$ (2.90 mmol) in 15 mL CH_3CN and $[\text{N}(\text{CH}_3)_4][\text{IO}_2\text{F}_4]$ (2.04 mmol) in 7 mL CH_3CN were combined inside a dry box in a 100 mL Teflon bottle. Instantaneously, a copious white precipitate formed that was pressure-filtered through a Teflon filter (Pall Corp). The white filtercake was transferred into a 3/4" o.d. Teflon ampoule equipped with a stainless steel valve and pumped to dryness for 2 h at ambient temperature. Vibrational spectroscopy of the filtercake showed the presence of $[\text{N}(\text{CH}_3)_4]_2[\text{IO}_2\text{F}_5]$, $[\text{N}(\text{CH}_3)_4][\text{cis-IO}_2\text{F}_4]$, and trace amounts of $[\text{N}(\text{CH}_3)_4][\text{trans-IO}_2\text{F}_4]$.

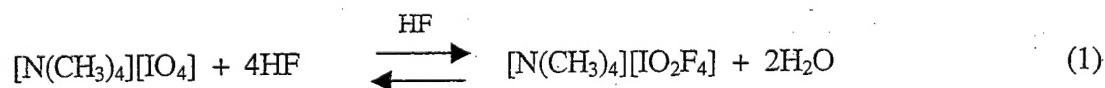
Raman Spectroscopy. The low-temperature spectra were recorded either with a Jobin-Yvon Model S-3000 spectrometer, using the 514.5 nm line of an Ar ion laser and an Olympus metallurgical microscope (model BHSM-L-2) for focusing the laser, a Cary Model 83GT with 488 nm excitation from an Ar ion laser, or a Spex Model 1403 with 647.1 nm excitation from a

Kr ion laser. Spectra were recorded at low temperature using microcrystalline samples of $[\text{N}(\text{CH}_3)_4]_2[\text{IO}_2\text{F}_5]$ / $[\text{N}(\text{CH}_3)_4][\text{cis-IO}_2\text{F}_4]$ sealed in Pyrex melting point capillaries.

Theoretical Calculations. Electronic structure calculations were done at the local density functional theory (LDFT)^{22,23} and the Hartree-Fock (HF) level.²⁴ The LDFT calculations were done with a polarized valence double ζ basis set (DZVP).²⁵ The HF calculations were done with a polarized valence double ζ basis set augmented by diffuse functions²⁶ on O and F and a polarized valence double ζ basis set on I with an effective core potential.²⁷ Geometries were optimized and second derivatives were calculated at the optimized geometries. The initial LDFT calculations were done with DGAUSS²⁸ (using the A1 charge fitting basis set) and the final LDFT and HF calculations were done with Gaussian 98.²⁹ The second derivatives were analyzed by using the program BMATRIX developed by Komornicki.³⁰ Raman intensities were determined analytically at the HF level and numerically at the LDFT level. Because we did not use a large basis set with diffuse functions to get accurate polarizabilities, the Raman intensities provide only qualitative information.

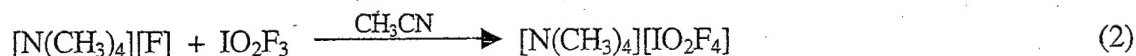
Results and Discussion

Synthesis of $[\text{N}(\text{CH}_3)_4][\text{IO}_2\text{F}_4]$. The $\text{N}(\text{CH}_3)_4^+$ salt of the known IO_2F_4^- anion was prepared by two synthetic routes. In analogy to the reported preparation of $[\text{Cs}][\text{IO}_2\text{F}_4]$,²⁰ a mixture of *cis*- and *trans*- $[\text{N}(\text{CH}_3)_4][\text{IO}_2\text{F}_4]$ in a 7 : 3 isomer ratio was obtained from $[\text{N}(\text{CH}_3)_4][\text{IO}_4]$ upon repeated treatments with a large excess of anhydrous HF (eq(1)).

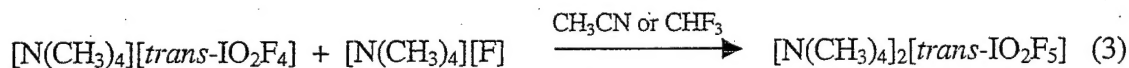


Alternatively, $[\text{N}(\text{CH}_3)_4][\text{IO}_2\text{F}_4]$ was synthesized by the reaction of IO_2F_3 with $[\text{N}(\text{CH}_3)_4][\text{F}]$ in

CH₃CN solution (eq (2)).



Synthesis of [N(CH₃)₄]₂[IO₂F₅]. A mixture of *cis*- and *trans*- [N(CH₃)₄][IO₂F₄] was allowed to react with one mole equivalent of [N(CH₃)₄][F] in CH₃CN either at -30 °C or at ambient temperature. The solvent was pumped off in a dynamic vacuum, yielding a white product consisting of [N(CH₃)₄]₂[*trans*-IO₂F₅] and [N(CH₃)₄][*cis*-IO₂F₄]. The reaction was also carried out in CHF₃ solution at 0 °C, but is less convenient due to the high vapor pressure of the solvent and the presence of some unreacted [N(CH₃)₄][*trans*-IO₂F₄] in the product. These results show that under the given reaction conditions only *trans*-IO₂F₄⁻ reacts with F⁻, yielding the *trans*-IO₂F₅²⁻ anion according to eq. (3).



The observation that exclusively the *trans*-IO₂F₄⁻ ion reacts with the F⁻ ion can be rationalized by kinetic effects. Because the oxygen double bond domains are larger and more repulsive than those of the fluorine single bonds,^{2,31} the F⁻ ion approaches the IO₂F₄⁻ ion in the direction of the least repulsion, i.e., through a triangular F₃ face in *cis*-IO₂F₄⁻, and through an F₂O face in *trans*-IO₂F₄⁻. In the latter case, the additional fluorine ligand can easily slip into the existing equatorial fluorine belt, resulting directly in the energetically favored *trans*-IO₂F₅²⁻ structure of *D*_{5h} symmetry. In the case of *cis*-IO₂F₄⁻, however, the analogous approach results in an intermediate structure that cannot easily rearrange to *D*_{5h} symmetry without the kinetically unfavorable, complete breakage and reformation of an I-F bond. This type of argument can also explain the lack of easy *cis/trans*-isomerization in pseudo-octahedral species, such as IO₂F₄⁻, and the ease of this isomerization in pseudo trigonal-bipyramidal species through a Berry pseudorotation mechanism.³²

Although most of the unreacted [N(CH₃)₄][*cis*-IO₂F₄] salt can be extracted from the

product mixture using CH_3CN , not all of the $[\text{N}(\text{CH}_3)_4][\text{cis-IO}_2\text{F}_4]$ was removed even after numerous washings. Removal of the solvent from the washings afforded isomerically pure $[\text{N}(\text{CH}_3)_4][\text{cis-IO}_2\text{F}_4]$, containing only some $[\text{N}(\text{CH}_3)_4][\text{F}]$, as shown by infrared spectroscopy. Although isomerically pure *trans*- IO_2F_4^- had previously been prepared,³³ this procedure represents the first isolation of isomerically pure *cis*- IO_2F_4^- .

Attempts to grow single crystals of $[\text{N}(\text{CH}_3)_4][\text{cis-IO}_2\text{F}_4]$ from the CH_3CN extract of the crude $[\text{N}(\text{CH}_3)_4]_2[\text{IO}_2\text{F}_5] / [\text{N}(\text{CH}_3)_4][\text{cis-IO}_2\text{F}_4] / [\text{N}(\text{CH}_3)_4][\text{F}]$ reaction product yielded crystals of $[\text{N}(\text{CH}_3)_4]_2[\text{IO}_2\text{F}_2][\text{HF}_2]$ instead.³⁴ The reducing agent required for the reduction of $\text{I(VII)O}_2\text{F}_4^-$ to $\text{I(V)O}_2\text{F}_2^-$ is most likely CH_3CN . Tetramethylammonium fluoride may play a crucial role in this reduction because it is known to readily abstract a proton from CH_3CN yielding the CH_2CN^- anion.¹⁷

Vibrational Spectra and Structure of the *trans*- $\text{IO}_2\text{F}_5^{2-}$ Anion. The Raman spectrum of $[\text{N}(\text{CH}_3)_4]_2[\text{IO}_2\text{F}_5]$ containing about 25 weight % of $[\text{N}(\text{CH}_3)_4][\text{cis-IO}_2\text{F}_4]$ is shown in Figure 1. The observed vibrational frequencies for $\text{IO}_2\text{F}_5^{2-}$ and their assignments based on the theoretical calculations are summarized in Table 1. After subtraction of the bands belonging to the $\text{N}(\text{CH}_3)_4^+$ cation,³⁵ the *cis*- IO_2F_4^- anion, and trace amounts of CH_3CN , four new Raman bands at 789, 517, 395, and 368 cm^{-1} and four new infrared bands at 847, 490, 390, and 330 cm^{-1} remain that can be assigned to the novel pentagonal-bipyramidal $\text{IO}_2\text{F}_5^{2-}$ anion of D_{5h} symmetry with the oxygen atoms in the two axial positions (see Figure 2).

A total of 18 vibrational modes are expected for the $\text{IO}_2\text{F}_5^{2-}$ anion of D_{5h} symmetry which span the irreducible representations $\Gamma = 2A_1' + 3E_1' + 2E_2' + 2A_2'' + E_1'' + E_2''$. Of the resulting 11 fundamental vibrations, five are Raman active ($2A_1'$, $2E_2'$, and E_1''), five are infrared active ($2A_2''$ and $3E_1'$), and the E_2'' mode is inactive. Of the expected five Raman and five infrared active vibrations, four were observed in each spectrum. The Raman band at 789 and the infrared band at 847 cm^{-1} represent the symmetric ($\nu_1(A_1')$) and antisymmetric ($\nu_3(A_2'')$) stretching modes of the axial IO_2 unit, respectively. Their large frequency separation and mutual exclusion establish beyond doubt the linearity, i.e., the *trans*-configuration, of the O-I-O group. For the *cis*-

configuration and the monocapped octahedral and monocapped trigonal prismatic geometries, the symmetric and the antisymmetric IO_2 stretching modes would be both Raman and infrared active. This conclusion is further supported by a comparison with the spectra of $\text{trans-IO}_2\text{F}_4^-$ in its $\text{N}(\text{CH}_3)_4^+$ salt, where the mutually exclusive IO_2 stretching modes were observed at 813 and 880 cm^{-1} .²⁰ The observed decreases in frequency from IO_2F_4^- to $\text{IO}_2\text{F}_5^{2-}$ are consistent with the greater I-O bond polarity in the $\text{IO}_2\text{F}_5^{2-}$ anion resulting from the increased negative formal charge in the dianion (see below).

Similarly, the Raman band at 517 cm^{-1} , which corresponds to the symmetric stretching mode, $\nu_2(\text{A}_1')$, of the five equatorial I-F bonds, is considerably lower in frequency than the corresponding band found at 571 cm^{-1} for the four I-F bonds in $\text{trans-IO}_2\text{F}_4^-$. The second Raman active IF_5 stretching mode, $\nu_9(\text{E}_2')$, was not observed because of its low intensity and interference with the 457 cm^{-1} band of $\text{N}(\text{CH}_3)_4^+$. The infrared active antisymmetric IF_5 stretching mode, $\nu_5(\text{E}_1')$, was observed as a very strong IR band at 490 cm^{-1} , in accord with the predicted frequency and intensity values. The Raman band at 368 cm^{-1} is assigned to the IO_2 rocking mode, $\nu_8(\text{E}_1'')$, of $\text{IO}_2\text{F}_5^{2-}$, in accord with its predicted frequency and high Raman intensity.^{11,12} The only remaining Raman band occurs at 395 cm^{-1} , in excellent agreement with the frequency predictions for the IF_5 scissoring mode, $\nu_{10}(\text{E}_2')$. Of the three expected infrared active deformation modes, the IO_2 scissoring mode, $\nu_6(\text{E}_1')$, and the IF_5 umbrella deformation mode, $\nu_4(\text{A}'')$, were observed at the expected frequencies. The remaining antisymmetric IF_5 in plane deformation mode, $\nu_7(\text{E}_1')$, was not observed because of its low frequency and predicted near zero infrared intensity. The observed vibrational spectra are in excellent agreement with the qualitative predictions and calculated frequencies for $\text{trans-IO}_2\text{F}_5^{2-}$ of D_{5h} symmetry and confirm the existence and symmetry of this novel anion beyond doubt.

The pentagonal-bipyramidal D_{5h} geometry of $\text{IO}_2\text{F}_5^{2-}$ is in accord with the VSEPR models² and with the structures previously established for IF_5^{2-} and IOF_5^{2-} .^{10,14} All three anions possess a pentagonal IF_5 plane with the two axial positions occupied by free valence electron pairs or oxygen atoms. This is in accord with the doubly bonded oxygen and the free valence electron pair domains

being more repulsive than those of the fluorine ligands² and, therefore, occupying the less crowded axial positions. In this manner, they achieve maximum avoidance.

It is interesting to examine the frequency trends for the pentagonal planar IF_5 group within the IF_7 , IOF_6^- , $\text{IO}_2\text{F}_5^{2-}$, IOF_5^{2-} , and IF_5^{2-} series. In the isoelectronic IF_7 , IOF_6^- , and $\text{IO}_2\text{F}_5^{2-}$ sequence, the oxidation state of iodine remains the same (+VII), whereas the axial fluorine ligands are stepwise replaced by formally negatively charged O ligands thereby increasing the overall negative charges. In the $\text{IO}_2\text{F}_5^{2-}$, IOF_5^{2-} , and IF_5^{2-} sequence, the axial oxygen ligands are stepwise replaced by free valence electron pairs, causing a stepwise reduction of the iodine oxidation state from +VII to +III.

As shown in Table 2, the IF_5 stretching modes are most strongly influenced by the ionic charges and the resulting polarity of the I-F bonds, and to a lesser extent by the replacement of oxygen by a free valence electron pair. Similarly, the IF_5 in-plane deformation frequencies decrease with an increase in the ionic charge, but change only little upon replacement of an oxygen ligand by a free valence electron pair, especially for the replacement of the second oxygen atom by a free valence electron pair. The out-of-plane deformation modes change much less. Apparently, the lengthening and weakening of the I-F bonds by their increasing polarity is counteracted by the increased repulsion resulting from the replacement of an axial fluorine ligand by either a more repelling oxygen ligand or an iodine free valence electron pair.

Although no main group D_{5h} AO_2X_5 species had previously been reported, the crystal structure³⁶ and infrared spectrum³⁷ of pentagonal-bipyramidal $\text{UO}_2\text{F}_5^{3-}$ were published in 1954 and 1968, respectively. A comparison of the vibrational frequencies and assignments listed³⁸ for $\text{UO}_2\text{F}_5^{3-}$ with those of *trans*- $\text{IO}_2\text{F}_5^{2-}$ casts serious doubts on the published vibrational analysis of $\text{UO}_2\text{F}_5^{3-}$. Particularly disturbing are the high frequencies attributed to the U-F stretching modes in this trianion.

Vibrational Spectra of $[\text{N}(\text{CH}_3)_4][\text{cis-IO}_2\text{F}_4]$. The availability of isomerically pure $[\text{N}(\text{CH}_3)_4][\text{cis-IO}_2\text{F}_4]$, of previous data for the isomerically impure cesium salt,²⁰ and of calculated frequencies and intensities permitted conclusive assignments for this anion (see Table 3). With the

exception of ν_6 and ν_{15} , which based on the theoretical predictions have vanishing infrared and Raman intensities, all fundamental vibrations can be assigned to the experimentally observed frequencies, assuming double coincidences for ν_5 / ν_{14} and ν_7 / ν_{11} , respectively. This assumption is supported by the theoretical calculations which predict that their frequencies are almost identical. The observed spectra are in accord with the theoretical predictions and those of the closely related *cis*-OsO₂F₄ molecule³⁹ which exhibits a very similar spectrum. The following geometry was calculated for *cis*-IO₂F₄⁻ at the HF/ECP/DZVP level of theory: I-O 1.731 Å; I-F_{ax} = 1.843 Å; I-F_{eq} = 1.856 Å; O-I-O = 104.4 °; O-I-F_{ax} = 95.3 °; O-I-F_{eq} = 89.3 °; F_{eq}-I-F_{eq} = 77.0 °; with the energy of the *cis*-isomer being 3.3 kcal/mol, 2.3 kcal/mol, and 1.8 kcal/mol higher than that of the *trans*-isomer at the HF/ECP, NLDFT, and LDFT levels of theory, respectively. The I-O and I-F bond lengths in the *cis*-isomer are very similar to those (I-O = 1.731 Å and I-F = 1.855 Å) of the *trans*-isomer at the same level of theory.

Theoretical Calculations

Normal Coordinate Analysis of *trans*-IO₂F₅²⁻. Because doubly charged anions, such as IO₂F₅²⁻, exhibit only very little solubility in common solvents and, in solution, revert to the singly charged anions and free fluoride, it was not possible to grow single crystals for x-ray diffraction. Therefore, theoretical calculations of the vibrational frequencies and intensities and their fit with the observed spectra were used to determine the structure of IO₂F₅²⁻ and to evaluate the structural trends resulting from changes in the formal ionic charge, the oxidation state and coordination number (CN) of iodine, and the replacement of of an oxygen ligand by either a free valence electron pair or a fluorine ligand. Because our previous work had shown that for closely related iodine and xenon compounds HF/ECP/DZVP and LDFT/DZVP calculations, after appropriate scaling, approximate the experimental values quite well, the same approach was chosen for the present study.

As shown in Table 1, the agreement between the observed and calculated frequencies and intensities is good for IO₂F₅²⁻, thus confirming its *D*_{5h} geometry (see Figure 2). Based on a general

comparison of calculated and experimental geometries for the closely related six-coordinated series IO_2F_4^- , IOF_4^- , IF_4^- , IOF_5 , IF_5 , and IF_6^+ and the seven-coordinated series $\text{IO}_2\text{F}_5^{2-}$, IOF_5^{2-} , IF_5^{2-} , IOF_6^- , IF_6^- , and IF_7 (see Figures 3 and 4, respectively), the following bond lengths are predicted for *trans*- $\text{IO}_2\text{F}_5^{2-}$: $r_{\text{I-F}} = 1.97 \text{ \AA}$ and $r_{\text{I-O}} = 1.78 \text{ \AA}$ (see Table 4).

In view of the importance of the vibrational spectra for the identification of the novel *trans*- $\text{IO}_2\text{F}_5^{2-}$ anion, a normal coordinate analysis was carried out using the scaled LDFT/DZVP frequencies from Table 1. The results are summarized in Table 5 and confirm the assignments and approximate mode descriptions given in Table 1. As can be seen from the Potential Energy Distribution (PED) in Table 5, all modes are highly characteristic, except for ν_6 and ν_7 which are symmetric and antisymmetric combinations, respectively, of the IO_2 scissoring and the IF_5 antisymmetric in plane deformation motions. The I-O and I-F stretching force constants have values of about 5.64 mdyn/\AA and 2.42 mdyn/\AA , respectively, and correlate well with the predicted bond distances.

Analysis of *cis*- $\text{IO}_2\text{F}_5^{2-}$. The stability of *cis*-isomers of $\text{IO}_2\text{F}_5^{2-}$ was also explored computationally at the LDFT/dzvp level of theory. Only one stable isomer was found which is shown in Figure 5. It possesses one axial and one equatorial oxygen atom and is 19.6 kcal/mol higher in energy than the *trans*-isomer. The equatorial oxygen ligand requires more space than the fluorine ligands and is displaced from the equatorial plane by about 20° . This displacement causes a tilt of the adjacent axial fluorine ligand by about 14° . The remaining $\text{F}_{\text{ax}}\text{IF}_4$ fragment of the ion is part of an almost perfect pentagonal bipyramid. The geometry and unscaled vibrational frequencies of the *cis*-isomer of $\text{IO}_2\text{F}_5^{2-}$ are summarized in Table 6. The poor correspondence between calculated and observed frequencies and intensities rules out the possibility of assigning the observed spectra to the *trans*-isomer.

General Trends. Figures 3 and 4 also allow us to study the influence of the coordination number and oxidation state of iodine and of the ionic charge on the structures of these species. Because the HF/ECP/DZVP bond lengths approximate the experimental values better than the LDFT/DZVP results, the former values were used. In spite of IF_6^- having in its $\text{N}(\text{CH}_3)_4^+$ salt a

monocapped octahedral structure,⁴⁰ a pseudopentagonal-bipyramidal structure was used for our study to allow a better comparison with the other members of this series. This is not unreasonable because the three possible structures, a monocapped octahedron, a pentagonal bipyramid, and a monocapped trigonal prism are very close in energy,^{1,41}

An analysis of these figures reveals the following effects.

(i): The hexa- and hepta-coordinated compounds exhibit similar general trends, except for the bonds in the hepta-coordinated compounds being longer than those in the hexa-coordinated ones. Whereas this difference is very pronounced for the equatorial iodine-fluorine bonds (~8-10 pm), it is much smaller (~1-2 pm) for the other bonds. Because in these two series the equatorial fluorine ligands preferentially form semi-ionic, multi-center bonds,^{9,42-44} they are much more susceptible to changes induced by hypervalency and increased bond ionicity.

(ii): The equatorial I-F bond lengths are most strongly influenced by the ionic charges of the ions and the oxidation state of the central iodine atom (see Figure 6). This is not surprising in view of Statement (i), because both, an increased negative charge and a reduced effective electronegativity of the central atom, increase the ionicity of the equatorial I-F bonds.

(iii): The axial I-F bonds are predominantly covalent and, therefore, similar in the hexa- and hepta-coordinated species. They also gain substantial ionicity from an increase in the ion charge (see Figure 7).

(iv): The axial I-O bonds are also similar in the hexa- and hepta-coordinated species, but are much less influenced by changes in either the ion charge or the oxidation state of the central atom (see Figure 8).

(v): As one might expect, the replacement of axial fluorine ligands by less electron withdrawing oxygen ligands and the replacement of oxygen ligands by electron feeding free valence electron pairs both decrease the effective electronegativity of the central atom and, thereby, increase the ionicity of the remaining I-F bonds. However, because these changes always go hand-in-hand with changes in the ion charge and the oxidation state of the central atom, they cannot be assessed independently in a more quantitative manner. The combination of these effects causes

IF_6^+ , with a positive ion charge, an iodine oxidation state of (VII), a CN of six, and no oxygen ligands or free iodine valence electron pairs, to exhibit the shortest I-F bond (1.75 Å), while IF_5^{2-} , with two negative ion charges, an iodine oxidation state of (III), a CN of seven, and two free iodine valence electron pairs, has the longest I-F bonds of 2.095 Å. This wide range in the I-F bond lengths is quite remarkable.

(vi): The O-I-F bond angles in IOF_4^- and IOF_5^{2-} , which contain one oxygen atom and one free valence electron pair in the two axial positions, provide information concerning the relative repulsion domains of doubly bonded oxygen and a sterically active free valence electron pair. In both ions, the O-I-F angle is somewhat larger than 90° , indicating that, in these compounds, the doubly bonded oxygen domain is slightly more repulsive than that of the free valence electron pair.

(vii): The experimentally observed bond distances (see Figures 3 and 4) are in accord with the calculated trends except for the axial I-F bond reported for IOF_5 .⁴⁵ The reported electron diffraction data did not permit an unambiguous determination of this distance and a redetermination of this structure by x-ray crystallography or other methods is called for. In accord with a previous study,¹¹ we predict that the axial bond length is about 1.815 Å, close to that of the equatorial I-F bonds.

(viii): The observed structures and bonding in these iodine fluorides and oxofluorides are in accord with previously proposed bonding models.^{3,9} Based on these models, the oxygen-iodine σ -bonds and the free valence electron pairs of iodine seek high s character by utilizing sp^n orbitals of the iodine atom, while the remaining fluorine ligands preferentially form highly ionic, multi-center bonds.^{3,9,42-44}

Conclusions

The fluoride ion acceptor properties of *cis*- IO_2F_4^- and *trans*- IO_2F_4^- have been studied. Because of an expected large activation energy barrier in a *cis*- IO_2F_4^- / F^- adduct toward rearrangement to the energetically favored D_{5h} *trans*- $\text{IO}_2\text{F}_5^{2-}$ structure, only the *trans*- IO_2F_4^- anion acts as a fluoride ion acceptor. The resulting novel *trans*- $\text{IO}_2\text{F}_5^{2-}$ anion has been isolated and characterized, and is presently the only known main-group $\text{AO}_2\text{F}_5^{n-}$ species. Based on its

vibrational spectra and electronic structure calculations, the $\text{IO}_2\text{F}_5^{2-}$ anion has the pentagonal-bipyramidal geometry preferred by main-group fluorides and oxofluorides with CN 7. An analysis of the calculated structures of six- and seven-coordinate iodine fluorides and oxofluorides reveals systematic trends that are dominated by changes in the ionicity of the I-F bonds due to the formal ionic charges of the species and the oxidation states of the central atom.

Acknowledgements

We thank the donors of the Petroleum Research Fund, administered by the American Chemical Society, for support of this work under ACS-PRF No. 28284-AC3 (G.J.S.). We also thank the National Science Foundation for the award of a NATO Postdoctoral Fellowship (W.J.C.). The work at USC was financially supported by the National Science Foundation and that at Edwards by the Air Force Office of Scientific Research and the Defense Advanced Research Projects Agency. One of us (M.G.) thanks the Ontario Ministry of Education and the Richard Fuller and James A. Morrison Memorial Funds for the award of graduate scholarships. A part of the work at PNL was supported by the Department of Energy. We thank Dr. Ross Wagner for his help with the preparation of some starting materials and Dr. Robert Syvret for his preparation of the IO_2F_3 sample.

References

*Authors to whom correspondence should be addressed. E-mail addresses:

karl.christe@edwards.af.mil; schrobil@mcmil.cif.mcmaster.ca; david.dixon@pnl.gov.

^{*}Loker Hydrocarbon Research Institute

[†]Air Force Research Laboratory

[‡]McMaster University

[§]Pacific Northwest National Laboratory

[¶]Present address: Department of Chemistry and Biochemistry, The University of Lethbridge, Lethbridge, Alberta, T1K 3M4, Canada.

- (1) Kepert, D. *Inorganic Stereochemistry*; Springer: Berlin, 1982.
- (2) Gillespie, R. J.; Hargittai, I. *The VSEPR Model of Molecular Geometry*; Allyn and Bacon, A Division of Simon & Schuster, Inc.: Needham Heights, MA, 1991; and Gillespie, R. J.; Popelier, P. L. A. *Chemical Bonding and Molecular Geometry: from Lewis to Electron Densities*; Oxford University Press, 2001.
- (3) Christe, K. O.; Curtis, E. C.; Dixon, D. A.; Mercier, H. P. A.; Sanders, J. C. P.; Schrobilgen, G. J.; Wilson, W. W. *Inorganic Fluorine Chemistry Toward the 21st Century*, ACS Symposium Series 555, American Chemical Society, Washington, DC, 1994, p 66.
- (4) Seppelt, K. *Inorganic Fluorine Chemistry Toward the 21st Century*, ACS Symposium Series 555, American Chemical Society, Washington, DC, 1994, p 56.
- (5) Christe, K. O.; Curtis, E. C.; Dixon, D. A. *J. Am. Chem. Soc.* **1993**, *115*, 1520.
- (6) Christe, K. O.; Dixon, D. A.; Sanders, J. C. P.; Schrobilgen, G. J.; Wilson, W. W. *J.*

- Am. Chem. Soc.* **1993**, *115*, 9461.
- (7) Christe, K. O.; Curtis, E. C.; Dixon, D. A. *J. Am. Chem. Soc.* **1993**, *115*, 9655.
- (8) Drake, G. W.; Dixon, D. A.; Sheehy, J. A.; Boatz, J. A.; Christe, K. O. *J. Am. Chem. Soc.* **1998**, *120*, 8392.
- (9) Christe, K. O.; Curtis, E. C.; Dixon, D. A.; Mercier, H. P. A.; Sanders, J. C. P.; Schrobilgen, G. J. *J. Am. Chem. Soc.* **1991**, *113*, 3351.
- (10) Christe, K. O.; Wilson, W. W.; Drake, G. W.; Dixon, D. A.; Boatz, J. A.; Gnann, R. *Z. J. Am. Chem. Soc.* **1998**, *120*, 4711.
- (11) Christe, K. O.; Dixon, D. A.; Mahjoub, A. R.; Mercier, H. P. A.; Sanders, J. C. P.; Seppelt, K.; Schrobilgen, G. J.; Wilson, W. W. *J. Am. Chem. Soc.* **1993**, *115*, 2696.
- (12) Christe, K. O.; Dixon, D. A.; Sanders, J. C. P.; Schrobilgen, G. J.; Wilson, W. W. *Inorg. Chem.* **1993**, *32*, 4089.
- (13) Christe, K. O.; Dixon, D. A.; Sanders, J. C. P.; Schrobilgen, G. J.; Tsai, S. S., Wilson, W. W. *Inorg. Chem.* **1995**, *34*, 1868.
- (14) Christe, K. O.; Wilson, W. W.; Dixon, D. A.; Boatz, J. A. *J. Am. Chem. Soc.* **1999**, *121*, 3382.
- (15) Christe, K. O.; Wilson, R. D.; Schack, C. J. *Inorg. Synth.* **1986**, *24*, 3.
- (16) (a) Christe, K. O.; Wilson, W. W.; Schack, C. J. *J. Fluorine Chem.* **1978**, *11*, 71; (b) Winfield, J. M. *J. Fluorine Chem.* **1984**, *25*, 91; (c) Emara, A. A. A.; Schrobilgen, G. *J. Inorg. Chem.* **1992**, *31*, 1323.
- (17) Christe, K. O.; Wilson, W. W.; Wilson, R. D.; Bau, R.; Feng, J.-a. *J. Am. Chem. Soc.* **1990**, *112*, 7619.
- (18) Engelbrecht, A.; Peterfy, P.; Schandara, E. Z. *Anorg. Allg. Chem.* **1971**, *384*, 202.
- (19) Wagner, R. I.; Bau, R.; Gnann, R. Z.; Jones, P. F.; Christe, K. O. *Inorg. Chem.* **1997**,

36, 2564.

- (20) Christe, K. O.; Wilson, R. D.; Schack, C. J. *Inorg. Chem.* **1981**, *20*, 2104.
- (21) Christe, K. O.; Schack, C. J.; Wilson, R. D.; *Inorg. Chem.* **1977**, *16*, 849.
- (22) (a) Parr, R. G.; Yang, W. *Density Functional Theory of Atoms and Molecules*. Oxford University Press, New York, **1989**; (b) Labanowski, J.; Andzelm, J., Eds. *Density Functional Methods in Chemistry*. Springer Verlag, New York, **1991**; (c) Ziegler, T. *Chem. Rev.* **1991**, *91*, 651; (d) Salahub, D. R. In *Ab Initio Methods in Quantum Chemistry -II*, Lawley, K. P., Ed. J. Wiley & Sons, New York. p. 447, **1987**; (e) Jones, R.O., Gunnarsson, O. *Rev. Mod. Phys.* **1989**, *61*, 689.
- (23) Vosko, S. J.; Wilk, L.; Nusair, W. *Can. J. Phys.* **1980**, *58*, 1200. (Keyword = SVWN5 in Gaussian 98).
- (24) (a) Hirst, D.M. "A Computational Approach to Chemistry" *Blackwell Scientific*, Oxford (1990); (b) Grant, G. H.; Richards, W.G. "Computational Chemistry" Oxford University Press, Oxford (1995); (c) Hehre, W.J.; Radom, L.; Schleyer, P.vR.; Pople, J.A. "Ab Initio Molecular Orbital Theory" John Wiley and Sons, New York (1986).
- (25) Godbout, N.; Salahub, D.R.; Andzelm, J.; Wimmer, E. *Can. J. Chem.* **1992**, *70*, 560. Basis sets were obtained from the Extensible Computational Chemistry Environment Basis Set Database developed in and distributed by the Molecular Science Computing Facility, William R. Wiley Environmental and Molecular Sciences Laboratory, Pacific Northwest National Laboratory.
<http://www.emsl.pnl.gov:2080/forms/basisform.html>.
- (26) Dunning, T.H., Jr.; Hay, P.J. in *Methods of Electronic Structure Theory*, Schaefer, H.F., III, Ed., Plenum Press: New York, **1977**, Ch. 1.
- (27) Hay, P.J.; Wadt, W. R. *J. Chem. Phys.* **1985**, *82*, 270, 284, 299.

- (28) (a) Andzelm, J.; Wimmer, E.; Salahub, D. R. in *The Challenge of d and f Electrons: Theory and Computation*; Salahub, D. R.; Zerner, M. C., Eds.; ACS Symposium Series, No. 394, American Chemical Society: Washington D. C., 1989; p228. (b) Andzelm, J. in *Density Functional Theory in Chemistry*; Labanowski, J.; Andzelm, J., Eds.; Springer-Verlag: New York, 1991, p 155. (c) Andzelm, J. W.; Wimmer, E. *J. Chem. Phys.* **1992**, *96*, 1280.
- (29) Frisch, M. J.; Trucks, G. W.; Schlegel, H. B.; Scuseria, G. E.; Robb, M. A.; Cheeseman, J. R.; Zakrzewski, V. G.; Petersson, G. A.; Montgomery, J. A., Jr.; Stratmann, R. E.; Burant, J. C.; Dapprich, S.; Millam, J. M.; Daniels, A. D.; Kudin, K. N.; Strain, M. C.; Farkas, O.; Tomasi, J.; Barone, V.; Cossi, M.; Cammi, R.; Mennucci, B.; Pomelli, C.; Adamo, C.; Clifford, S.; Ochterski, J.; Petersson, G. A.; Ayala, P. Y.; Cui, Q.; Morokuma, K.; Malick, D. K.; Rabuck, A. D.; Raghavachari, K.; Foresman, J. B.; Cioslowski, J.; Ortiz, J. V.; Stefanov, B. B.; Liu, G.; Liashenko, A.; Piskorz, P.; Komaromi, I.; Gomperts, R.; Martin, R. L.; Fox, D. J.; Keith, T. A.; Al-Laham, M. A.; Peng, C. Y.; Nanayakkara, A.; Gonzalez, C.; Challacombe, M.; Gill, P. M. W.; Johnson, B. G.; Chen, W.; Wong, M. W.; Andreas, J. L.; Head-Gordon, M.; Replogle, E. S.; Pople, J. A. Gaussian 98, A.7, Gaussian, Inc. Pittsburg PA, 1998.
- (30) BMATRIX Version 2.0; Kormonicki, A.; Polyatomics Research Institute: Palo Alto, CA, 1996.
- (31) Gillespie, R. J.; Robinson, E. A. *Angew. Chem. Int. Ed. Engl.* **1996**, *35*, 495.
- (32) Berry, R. S. *J. Chem. Phys.* **1960**, *32*, 933.
- (33) Gillespie, R. J.; Krasznai, J. P. *Inorg. Chem.* **1977**, *16*, 1384.
- (34) Gerken, M. Ph. D. Thesis, McMaster University, Hamilton, ONT. 2001.

- (35) Berg, R. W. *Spectrochim. Acta, Part A* **1978**, 34A, 655.
- (36) Zachariasen, W. H. *Acta Crystallogr.* **1954**, 7, 783.
- (37) Nguyen-Quy-Dao, *Bull. Soc. Chim. Fr.* **1968**, 3976.
- (38) Nakamoto, K. *Infrared and Raman Spectra of Inorganic and Coordination Compounds, Part A*; John Wiley and Sons, Inc. New York, Fifth Ed. 1997, p 228.
- (39) Christe, K. O.; Dixon, D. A.; Mack, H. G.; Oberhammer, H.; Pagelot, A.; Sanders, J. P. G.; Schrobilgen, G. J. *J. Am. Chem. Soc.* **1993**, 115, 11279.
- (40) Mahjoub, A.-R.; Seppelt, K. *Angew. Chem., Int. Ed. Engl.* **1991**, 30, 323.
- (41) Mahjoub, A.-R.; Drews, T.; Seppelt, K. *Angew. Chem., Int. Ed. Engl.* **1992**, 31, 1036.
- (42) Pimentel, G. C. *J. Chem. Phys.* **1951**, 19, 446.
- (43) Hach, R. J.; Rundle, R. E. *J. Am. Chem. Soc.* **1951**, 73, 4321.
- (44) Rundle, R. E. *J. Am. Chem. Soc.* **1963**, 85, 112.
- (45) Bartell, L. S.; Clippard, F. B.; Jacob, E. J. *Inorg. Chem.* **1976**, 15, 3009.

Table 1. Observed and Calculated Vibrational Spectra of the *trans*-IO₂F₅²⁻ Anion and their Assignment in Point Group *D*_{5h}

assignt (activity)	approx mode description	obsd freq, cm ⁻¹ Raman ^{a,b}	(rel intensity) for [N(CH ₃) ₄] ₂ [IO ₂ F ₅] Infrared ^{c,d}	scaled ^f calcd freq, cm ⁻¹ (Ir, Ra intens) LDFT/DZVP HF/ECVP/DZVP
A ₁ ' (Ra)	ν ₁ , ν sym IO ₂	789 [100]	-	781(0) [37] 776 (0) [43]
	ν ₂ , ν sym IF ₅	517 [57]	-	505 (0) [29] 505 (0) [27]
A ₂ " (IR)	ν ₃ , ν as IO ₂	-	847 s ^e	856 (150) [0] 861 (90) [0]
	ν ₄ , δ umbrella IF ₅	-	330 m, sh ^e	338 (40) [0] 352 (86) [0]
E ₁ ' (IR)	ν ₅ , ν as IF ₅	-	490 vs	537 (591) [0] 503 (808) [0]
	ν ₆ , δ scissoring IO ₂	-	390 s	389(97) [0] 391 (291) [0]
	ν ₇ , δ as IF ₅ in plane	-	not obsd	244 (0) [0] 251 (0) [0]
E ₁ " (Ra)	ν ₈ , δ rock IO ₂	368 [57]	-	340 (0) [13] 346 (0) [14]
E ₂ ' (Ra)	ν ₉ , ν as IF ₅	not obsd ^g	-	449 (0) [4] 442 (0) [0.6]
	ν ₁₀ , δ scissoring IF ₅	395 [26] ^e	-	393 (0) [7] 392 (0) [3.8]
E ₂ " (i.a.)	ν ₁₁ , δ puckering IF ₅	-	-	158 (0) [0] 176 (0) [0]

^a Spectrum recorded on microcrystalline solid in a Pyrex glass capillary at -113 °C using the 514.5-nm excitation. ^b The N(CH₃)₄⁺ cation modes were observed at 380 (11), ν₈(E); 457 (13), ν₁₀(F₂); 752 (35), ν₃(A₁); 953 (22), ν₁₈(F₂); 1187 (3), ν₁(E); 1294 (3), ν₁₇(F₂); 1418 (5), ν₁₀(F₂); 1465 sh, ν₂(A₁); 1476 (31), ν₆(E); 2818 (4), 2828 (5), 2836 (5), 2899 sh, 2934 (16), 2970 (25), 2995 (15), 3038 (33) cm⁻¹, ν_{CH3} and binary bands (see refs 17 and 33). The *cis*-IO₂F₄⁻ anion modes were observed at 209 (1), 331 (14), 356(3)sh, bending modes;

395(26), $\nu_4(A_1)$; 567 (7), $\nu_3(A_1)$; 608 (26), $\nu_2(A_1)$; 854 (31), $\nu_1(A_1)$; 871 (5), $\nu_{12}(B_2)$ (see ref 20 and Table 3). Bands arising from residual CH_3CN were observed at 916 (7), $\nu_4(A_1)$; 1378 (1), $\nu_3(A_1)$; 2247 (14), $\nu_2(A_1)$; 2944 (16) cm^{-1} , $\nu_1(A_1)$.^d The $\text{N}(\text{CH}_3)_4^+$ cation modes were observed at 462 sh, $\nu_{19}(\text{F}_2)$; 922 w, $2\nu_{19}$; 955 vs, $\nu_{18}(\text{F}_2)$; 1257 mw, 1265 mw, $\nu_{17}(\text{F}_2)$; 1420 m, $\nu_{16}(\text{F}_2)$; 1497 s, $\nu_{15}(\text{F}_2)$; 1774 w, br, 1943 w, vbr, 2340 w, 2362 w, 2499 w, 2589 w, 2998 m, 3046 s, 3411 vw, 3493 vw cm^{-1} , ν_{CH_3} and binary bands (see refs 17 and 35). The $\text{cis-IO}_2\text{F}_4^-$ anion modes were observed at 354 vs; 367 vs, $\nu_5(A_1)$; 564 sh, $\nu_3(A_1)$; 620 vs, br, $\nu_2(A_1)$ and $\nu_9(B_1)$; 847 vs, $\nu_1(A_1)$; 871 vs, $\nu_{12}(B_2)$ (see ref 20 and Table 3).^e These $\text{IO}_2\text{F}_5^{2-}$ anion bands overlap with bands of the $\text{cis-IO}_2\text{F}_4^-$ anion.^f The following empirical scaling factors were used to obtain the best fit with the observed frequencies: LDFI, I-O stretching modes, 1.1081; HF, I-O stretching modes, 1.0436; remaining modes, 0.9388.^g Obscured by the 457 cm^{-1} Raman band of $\text{N}(\text{CH}_3)_4^+$.

Table 2. Comparison of the Vibrational Frequencies of the Pentagonal Planar IF_5 part in *trans*- IO_2F_3 with those of IF_7 , IOF_6^- , IOF_5^- , IOF_3^- , and IF_5^- in Point Group C_{5v}

assignt	approx mode description	+VII — replacem. of F by O ⁺ IF_7 [5]	+VII — replacem. of F by O ⁺ IOF_6^- [11]	+VII — replacem. of O by free valence el. pair — IO_2F_3^-	+V — replacem. of O by free valence el. pair — IOF_5^- [14]	+III — replacem. of O by free valence el. pair — IF_3^- [10]
		IF_7 [5]	IOF_6^- [11]	IO_2F_3^-	IOF_5^- [14]	IF_3^- [10]
A_1	ν sym IF_5	635	584	517	485	474
	δ umbrella IF_5	365	359	330	289	[307] ^a
E_1	ν asym IF_5	670	585	490	334	335
	δ as IF_5 in plane	425	405	[250]	254	245
E_2	ν asym IF_5	596	530	[450]	367/355	339/325
	δ scissoring IF_5	510	457	395	409	396
	δ puckering IF_5	[68]	[59]	[160]	[115]	[100]

^a Values in brackets are calculated frequencies.

Table 3. Observed and Calculated Vibrational Spectra of the *cis*-IO₂F₄ Anion and their Assignment in Point Group C_{2v}

assignt (activity)	approx mode description	obsd freq, cm ⁻¹ (rel intensity)				scaled ^b calcd freq, cm ⁻¹ (Ir, Ra intens)			
		Raman (solid)	Infrared (solid)	CsIO ₂ F ₄ ^a	Raman (solid)	Infrared (solid)	Raman (CH ₃ CN sol)	LDFT/DZVP	HF/ECP/DZVP
A ₁ (IR,Ra)	ν ₁ , ν sym IO ₂	847 [100]	844 s	856 [100]	855 vs	851 [90] p	863 (73) [22]	868 (87) [29.9]	
	ν ₂ , sym comb of ν sym IF _{2eq} and ν sym IF _{2ax}	608 [85]	605 s	605 [98]	600 vs, br	609 [100] p	593 (106) [30]	612 (134) [26.1]	
	ν ₃ , asym comb of ν sym	560 [24]	565 sh	552 sh	560 vw	540 [100] p	542 (0) [11]	556 (6) [6.3]	
	IF _{2eq} and ν sym IF _{2ax}								
	ν ₄ , δ sciss IO ₂	394 [15]	393 vw	394 [34]	395 sh	^c	377 (0) [4.6]	383 (20) [2.2]	
	ν ₅ , sym comb of δ sciss	370 [20]	370 s	369 [30]	364 s	355 sh ^c	366 (41) [3.2]	364 (92) [4.4]	
	IF _{2eq} and δ sciss IF _{2ax}								
	ν ₆ , asym comb of δ sciss	207 [3]		210 [0.5]			208 (0) [0.13]	227 (0.1) [0.1]	
	IF _{2eq} and δ sym IF _{2ax}								
A ₂ (-,Ra)	ν ₇ , torsion IO ₂	330 [38]	329 vw	332 [65]	328 w	335 sh	294 (0) [3.3]	320 (0) [3.4]	
	ν ₈ , torsion IF _{2eq}						172 (0) [0.1]	196 (0) [0.1]	
B ₁ (IR,Ra)	ν ₉ , ν as IF _{2ax}	610 ^d	613 vs		600 vs, br		614 (205) [1.1]	615 (280) [1.3]	

ν_{10} , δ rock IO_2	353 s	350 s	341 (35) [1.3]	360 (94) [0.9]
ν_{11} , δ rock $\text{IF}_{2\text{eq}}$	330 [38]	329 vw	332 [65]	321 (1) [2.5]
B_2 (IR,Ra) ν_{12} , ν as IO_2	868[7]	868 vs	875 ^d	884 (114) [6.7]
ν_{13} , ν as $\text{IF}_{2\text{eq}}$		555 m		885 (122) [9.0]
ν_{14} , sym comb of δ sciss	370 [20]	370 s	365 sh	551 (32) [3.3]
OIF _e and FIF _{ax}				533 (41) [1.6]
ν_{15} , asym comb of δ sciss		364 s	355 sh ^c	365 (48) [0.70]
OIF _e and FIF _{ax}				371 (115) [0.6]
				209 (0) [0.002]
				227 (0) [0]

^aData from ref 20. ^bEmpirical scaling factors of 1.06 and 1.122 were used for the LDFT stretching and deformation modes, respectively, to maximize the fit between observed and calculated frequencies; for the HH/ECP frequencies, scaling factors of 1.0, 0.9238, and 0.8615 were used for the IO stretching, the IF stretching, and the deformations modes, respectively. ^cInterference from a strong solvent band. ^dIntensities were omitted because of coincidences with other modes which contribute more strongly to the intensity.

Table 4. Calculated Unscaled and Predicted Geometries for $\text{IO}_2\text{F}_5^{2-}$

	HF/ECP/DZVP	LDFT/DZVP	predicted
R(I-F), Å	1.948	2.057	1.97
R(I-O), Å	1.751	1.824	1.78
∠F-I-O, deg	90	90	90
∠F-I-F, deg	72	72	72

Table 5. Symmetry Force Constants^a and Potential Energy Distribution^b of D_{5h} $\text{IO}_2\text{F}_5^{2-}$ Calculated from the Scaled^c LDFT/DZVP Second Derivatives

	freq, cm^{-1}		sym force constants	PED
	obsd	calcd		
A_1'	789	781	$F_{11} = 5.74$	100 (1)
			$F_{12} = 0.128$	
	517	505	$F_{22} = 2.86$	100 (2)
A_2''	847	856	$F_{33} = 5.54$	95 (3)
			$F_{34} = 0.225$	
	330	338	$F_{44} = 1.70$	100 (4)
E_1'	490	537	$F_{55} = 2.45$	90 (5), 7 (6), 2(8)
			$F_{56} = -0.521$	
			$F_{57} = 0.195$	
	390	389	$F_{66} = 2.45$	78 (6), 21 (7)
			$F_{67} = -0.450$	
	-	244	$F_{77} = 1.18$	58 (6), 41 (7)
E_1''	368	340	$F_{88} = 0.947$	100 (8)
E_2'	-	449	$F_{99} = 2.18$	88 (9), 12 (10)
			$F_{9,10} = 0.194$	
	395	393	$F_{10,10} = 2.11$	84 (10), 15 (9)
E_2''	-	158	$F_{11,11} = 0.598$	100 (11)

^a Stretching constants in $\text{mdyn}/\text{\AA}$, deformation constants in $\text{mdyn}\text{\AA}/\text{rad}^2$, and stretch-bend interactions constants in mdyn/rad . The force constants were scaled with the square of the scaling factors used for the corresponding frequencies. ^b PED in percent; symmetry coordinates: $S_1 = \nu$ sym IO_2 ; $S_2 = \nu$ sym IF_5 ; $S_3 = \nu$ asym IO_2 ; $S_4 = \delta$ umbrella IF_5 ; $S_5 = \nu$ asym IF_5 ; $S_6 = \delta$ scissoring IO_2 ; $S_7 = \delta$ asym IF_5 in plane; $S_8 = \delta$ rock IO_2 ; $S_9 = \nu$ asym IF_5 ; $S_{10} = \delta$ scissoring IF_5 ; $S_{11} = \delta$ puckering IF_5 .

Table 6. Geometry and Unscaled Vibrational Frequencies (Infrared Intensities) of the *cis*-isomer of $\text{IO}_2\text{F}_5^{2-}$ Calculated at the LDFT/DZVP Level of Theory in Point Group C_s

freq, cm^{-1} (IR intens)	geometry	
a' 780.6 (123)	R(I-O2)	1.846
734.5 (86)	R(I-O3)	1.830
477.0 (135)	R(I-F4)	2.038
439.4 (30)	R(I-F5)	2.100
422.3 (0.25)	R(I-F7)	2.066
372.9 (5.7)		
337.4 (66)	$\angle(\text{O2-I-O3})$	110.0
323.3 (37)	$\angle(\text{O2-I-F4})$	85.2
303.9 (4.4)	$\angle(\text{O2-I-F5})$	78.0
224.2 (0.03)	$\angle(\text{O3-I-F5})$	89.6
91.3 (0)	$\angle(\text{O3-I-F7})$	91.2
	$\angle(\text{F4-I-F5})$	93.7
a" 455.5 (258)	$\angle(\text{F4-I-F7})$	76.3
423.0 (2.2)	$\angle(\text{F5-I-F7})$	68.4
367.9 (72)	$\angle(\text{F7-I-F8})$	69.1
350.3 (1.3)		
282.3 (0.08)		
205.7 (0.03)		
28.5 (0.08)		

Diagram Captions

Figure 1. The Raman spectrum of $[\text{N}(\text{CH}_3)_4]_2[\text{IO}_2\text{F}_5]$ containing about 25 weight % of $[\text{N}(\text{CH}_3)_4][\text{cis-IO}_2\text{F}_4]$, recorded at $-113\text{ }^\circ\text{C}$ using 514.5 nm excitation. The *trans*- $\text{IO}_2\text{F}_5^{2-}$, *cis*- IO_2F_4^- , and $\text{N}(\text{CH}_3)_4$ bands are indicated by \ddagger , $*$, and \bullet respectively.

Figure 2. D_{3h} geometry of the *trans*- $\text{IO}_2\text{F}_5^{2-}$ anion.

Figure 3. Geometries of the hexacoordinated IO_2F_4^- , IOF_4^- , IF_4^- , IOF_5 , IF_5 , and IF_6^+ ions and molecules, calculated at the HF/ECP/DZVP level of theory. The calculated bond lengths and bond angles are given in bold and regular fonts, respectively, and the experimentally observed values are shown in brackets.

Figure 4. Geometries of the heptacoordinated $\text{IO}_2\text{F}_5^{2-}$, IOF_5^{2-} , IF_5^{2-} , IOF_6^- , IF_6^- , and IF_7 ions and molecules, calculated at the HF/ECP/DZVP level of theory. The calculated bond lengths and bond angles are given in bold and regular fonts, respectively, and the experimentally observed values are shown in brackets.

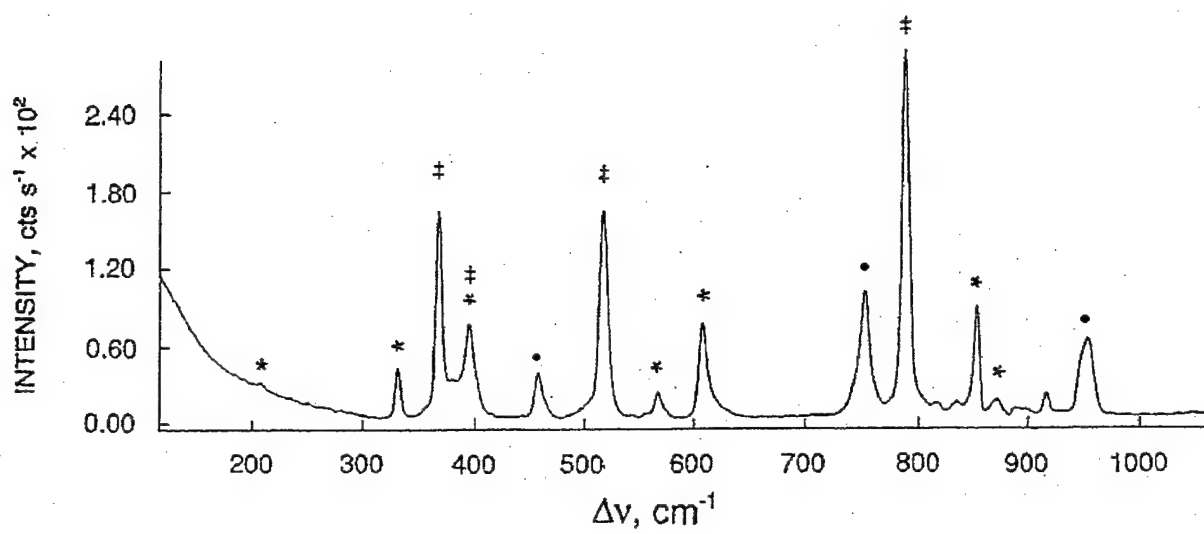
Figure 5. Minimum energy structure of *cis*- $\text{IO}_2\text{F}_5^{2-}$ calculated at the LDFT/DZVP level.

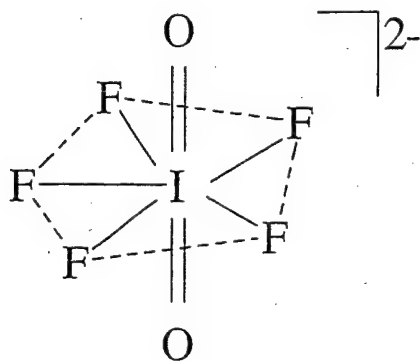
Figure 6. Changes of the equatorial I-F bond lengths with increasing formal ion charge and decreasing oxidation state of the central iodine atom. The arrangement of the individual compounds is identical to those in Figures 3 and 4, and the italic and regular numbers represent the hexa- and hepta-coordinated species, respectively.

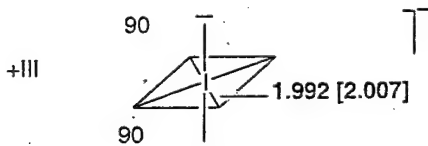
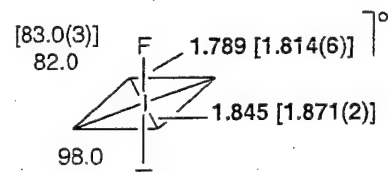
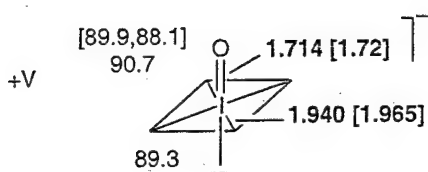
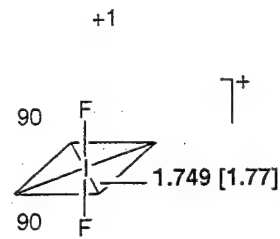
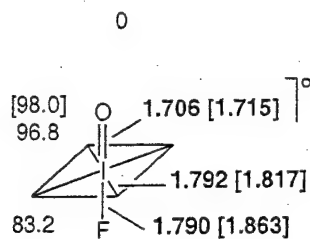
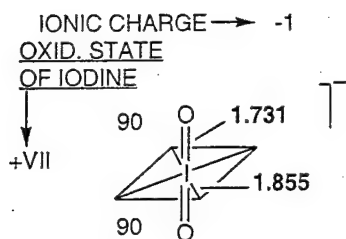
Figure 7. Changes of the axial I-F bond lengths with increasing ion charge and decreasing oxidation state of the central iodine atom. Italic and regular font numbers represent the hexa- and hepta-coordinated species, respectively.

Figure 8. Changes of the axial I-O bond lengths with increasing ion charge and decreasing oxidation state of the central iodine atom. Italic and regular font numbers repre-

sent the hexa- and hepta-coordinated species, respectively.

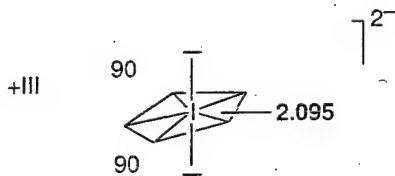
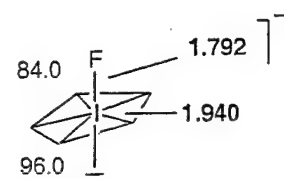
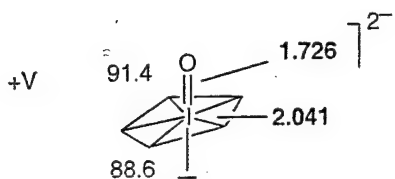
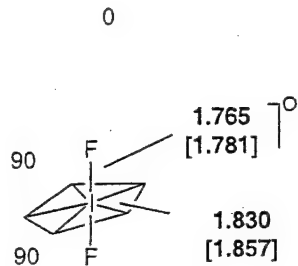
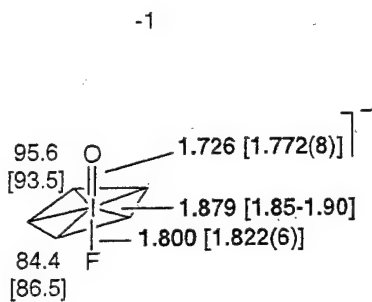
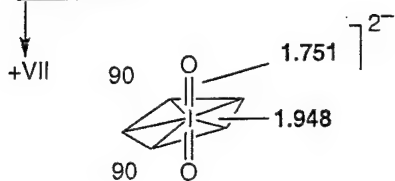




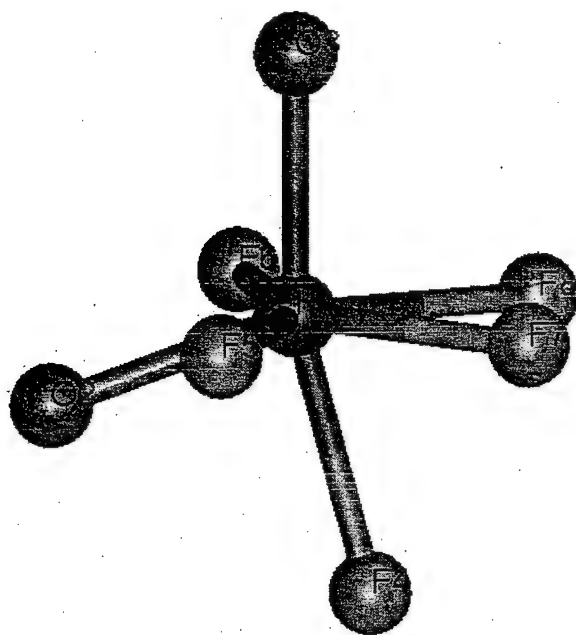


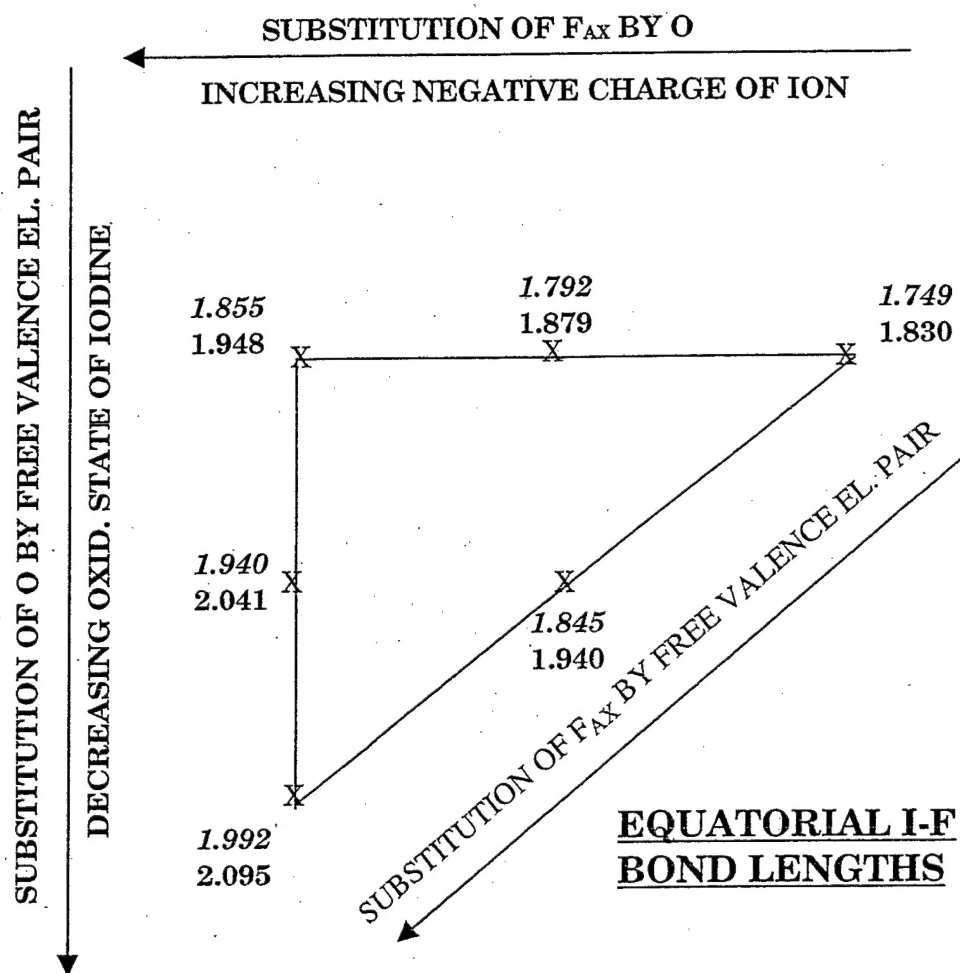
CN 6

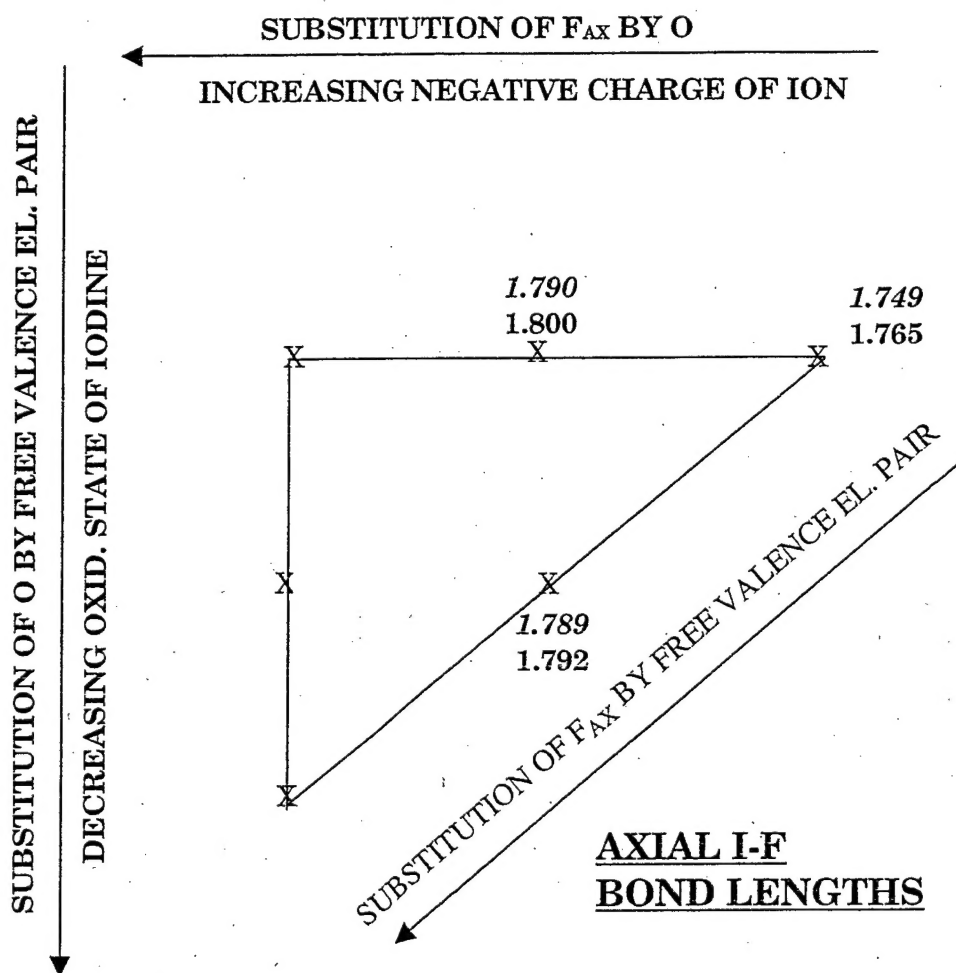
IONIC CHARGE → -2
 OXID. STATE
 OF IODINE

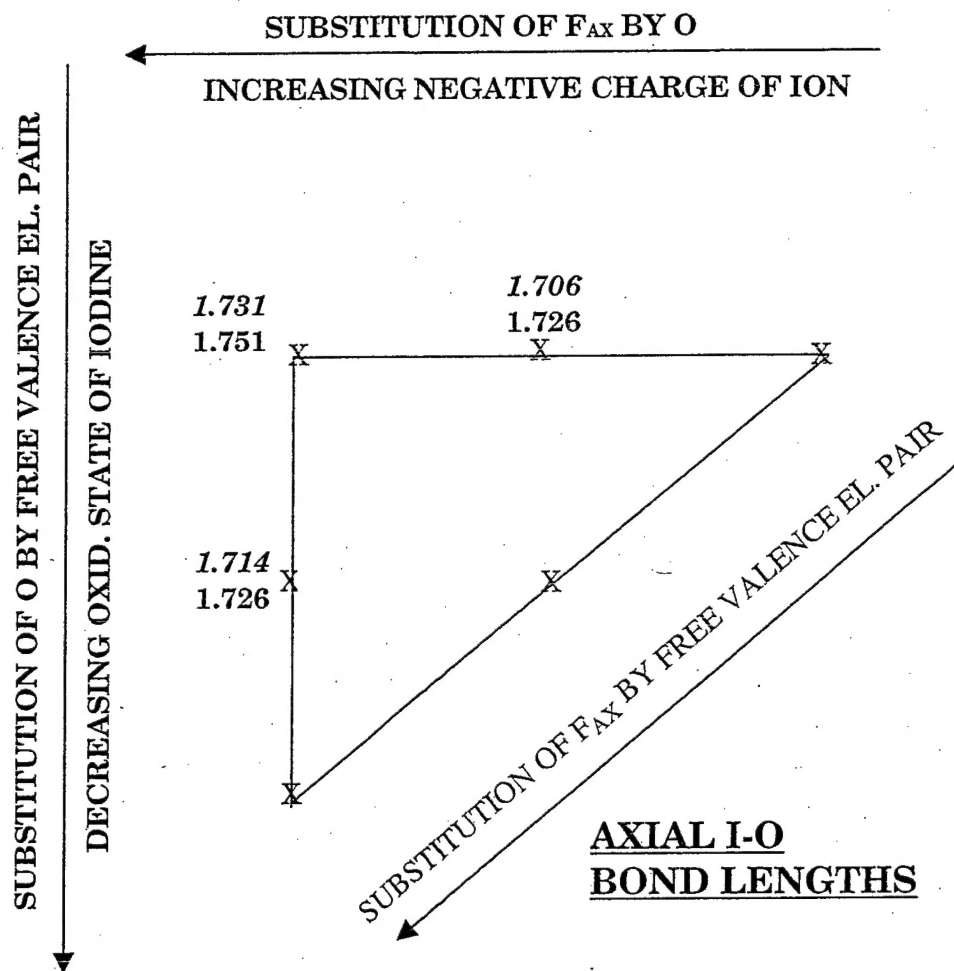


CN 7









Synthesis and Characterization of the *trans*-IO₂F₅²⁻ Dianion

Jerry A. Boatz, William J. Casteel, Jr., Karl O. Christe,*

David A. Dixon, Michael Gerken, Robert Z. Gnann,

Helène P. A. Mercier, and Gary J. Schrobilgen*

